Research Square

Preprints are preliminary reports that have not undergone peer review.
They should not be considered conclusive, used to inform clinical practice,
or referenced by the media as validated information.

Spatio-temporal characterisation of meteorological drought in selected districts in Tanzania: a multi-timescale analysis of trends, 1995-2024

Elia Magwaja

emagwaja@gmail.com

University of Dar es Salaam

Peter Tuju

Tanzania Meteorological Authority

Habiba Mtongori

Tanzania Meteorological Authority

Jim Todd

National Institute for Medical Research

Anthony Kapesa

Catholic University of Health and Allied Sciences

George PrayGod

National Institute for Medical Research

Brenda Kitilya

National Institute for Medical Research

Eliud Kamala

National Institute for Medical Research

Eliakimu Kapyolo

National Institute for Medical Research

Daniel Faurholt-Jepsen

Rigshospitalet

Zvifadzo Matsena Zingoni

UCLA David Geffen School of Medicine

Ladislaus Chang'a

Tanzania Meteorological Authority

Research Article

Keywords: Meteorological drought, Standardized Precipitation Index, Spatio-temporal analysis, Climate and health, Indian Ocean Dipole, Tanzania

Posted Date: November 24th, 2026

DOI: https://doi.org/10.21203/rs.3.rs-11677413/v1

License: This work is licensed under a Creative Commons Attribution 4.0 International License.
Read Full License

Additional Declarations: No competing interests reported.

Spatio-temporal characterisation of meteorological drought in selected districts in Tanzania: a multi-timescale analysis of trends, 1995-2024

Elia Magwaja[1,2,3], Peter Tuju[4], Habiba Mtongori[4], Jim Todd[2,3], Anthony Kapesa[3], George PrayGod[2,5], Brenda Kitilya[2], Eliud Kamala[2,3], Eliakimu Kapyolo[2,3], Daniel Faurholt-Jepsen[6,7], Zvifadzo Matsena Zingoni[8], Ladislaus Chang'a[9]

[1] College of Social Sciences, University of Dar es Salaam, Dar es Salaam, Tanzania

[2] Mwanza Research Centre, National Institute for Medical Research, Mwanza, Tanzania

[3] School of Public Health, Catholic University of Health and Allied Sciences, Mwanza, Tanzania

[4] Tanzania Meteorological Authority, Dar es Salaam, Tanzania

[5] Muhimbili Medical Research Centre, National Institute for Medical Research, Dar es Salaam, Tanzania

[6] Department of Infectious Disease, Rigshospitalet, Copenhagen, Denmark

[7] Department of Clinical Medicine, University of Copenhagen, Copenhagen, Denmark

[8] Center for Biomedical Modeling, Semel Institute for Neuroscience & Human Behavior, Department of Psychiatry, UCLA David Geffen School of Medicine, Los Angeles, CA, USA

[9] Tanzania Meteorological Authority, Dodoma, Tanzania

Corresponding author: Elia Magwaja, emagwaja@gmail.com

Acknowledgements

The authors would like to thank the Tanzania Meteorological Authority (TMA) for extracting the district rainfall series.

Abstract

District-scale drought characterisation is needed to study how climate variability affects health. We characterised meteorological drought in eight Tanzanian districts with contrasting rainfall regimes over 1995-2024 using the Standardized Precipitation Index (SPI) at 1-, 3-, 6- and 12-month timescales, computed from Climate Hazards Group InfraRed Precipitation with Station data (CHIRPS) and matched to each rainy season. We assessed drought frequency, run-theory events, copula return periods, trends with window sensitivity and false-discovery-rate (FDR) control, grid-cell (0.05°) patterns and links with the El Niño-Southern Oscillation (ENSO) and the Indian Ocean Dipole (IOD). No significant differences in severe-drought frequency were detected between districts (Monte-Carlo p = 0.43-0.84), and drought-prone districts did not experience severe drought more often. Drought was regionally coherent, with widespread events in 1996-2000, 2003-2006 and 2016-2017. Estimated SPI trends were positive in all eleven district-seasons (significant in four after FDR adjustment), no grid cell showed significant drying, and SPI-6 drought months fell from 736 in 1995-2009 to 235 in 2010-2024, but trend significance depended largely on the predominantly wet years 2019-2024. The IOD was the climate mode most strongly associated with October-December and November-April drought (r = 0.59-0.81), ENSO showed no significant independent association, and no severe drought occurred under a positive IOD; March-May drought was not significantly related to either mode. For drought-health studies, the results favour continuous, season-matched SPI over drought-prone labels, within-district comparisons with control for secular trends, separate treatment of the bimodal seasons, and evaluation of the IOD as a potential predictor.

Keywords: Meteorological drought, Standardized Precipitation Index, Spatio-temporal analysis, Climate and health, Indian Ocean Dipole, Tanzania

1 Introduction

Drought is a slow-onset hazard whose impacts on water supply, agriculture and livelihoods accumulate over months to years (Wilhite and Glantz 1985; Mishra and Singh 2010). It also affects health, through food insecurity and undernutrition, water-related and vector-borne diseases, and mental distress (Stanke et al. 2013; Vins et al. 2015; Salvador et al. 2023), and may disrupt the management of chronic conditions such as hypertension and diabetes through interrupted access to medicines and changes in diet (Moreira et al. 2024). Studies of these effects depend on how drought exposure is measured. Exposure has been measured in different ways, for example from disaster records, by labelling places as drought-prone, or with a drought index at a single timescale. The method chosen can change the results (Berman et al. 2017). Misclassified exposure also biases effect estimates towards the null (Armstrong 1998).

Meteorological drought, a precipitation deficit relative to local climatology, precedes and propagates into agricultural and hydrological drought (Van Loon 2015). It is usually measured with the Standardized Precipitation Index (SPI; McKee et al. 1993). The World Meteorological Organization recommends SPI for its simplicity, minimal data requirements, and flexibility across multiple timescales (Svoboda et al. 2012). In Tanzania the choice of timescale is important, because two rainfall regimes coexist: a unimodal November-April season and a bimodal regime with March-May (MAM) and October-December (OND) seasons (Nicholson 2017). Interannual rainfall variability in East Africa is influenced by large-scale climate modes, particularly the El Niño-Southern Oscillation (ENSO) and the Indian Ocean Dipole (IOD; Saji et al. 1999). These modes are strongly associated with variability in the October-December short rains, whereas their relationship with the March-May long rains is generally weaker and less consistent (Black et al. 2003; Behera et al. 2005; Nicholson 2017).

Drought research in Tanzania has examined rainfall trends from CHIRPS (Muthoni et al. 2019), the performance of drought indices and event definitions in individual river basins (Wambura 2025; Mukama et al. 2025), national drought patterns and their links with ENSO and the IOD up to 2016 (Makula et al. 2025), and future projections (Salah et al. 2023). Three limitations restrict the use of such work for health research. First, drought frequencies are commonly compared between locations, but since SPI is standardised separately at each location, observed differences may simply reflect random variation, especially when only 30 years of data are available. Second, trends estimated from short records can depend on the period analysed, and the serial correlation of overlapping SPI accumulations inflates the significance of standard trend tests (Hamed and Rao 1998). In addition, gridded trend maps are rarely corrected for multiple testing (Wilks 2016). Third, the observational studies do not extend beyond 2022, and most end before 2019. Subsequent years included exceptionally wet seasons: the 2019 short rains, associated with a strong positive IOD event (Wainwright et al. 2021), and the 2023/24 November-April season, the wettest in Tanzania since 1970, to which El Niño and positive IOD conditions contributed in early 2024 (TMA 2025). It therefore remains unclear whether observed changes in drought conditions reflect a long-term trend or short-term climate variability. Furthermore, these studies provide limited guidance on how drought exposure should be characterised for health research.

This study characterises the spatio-temporal patterns of meteorological drought from 1995 to 2024 in eight districts of mainland Tanzania representing contrasting rainfall regimes, selected within the Climate Change and Health in Tanzania (CLIMATCH) project. Using SPI at multiple timescales, with seasonal analyses matched to each district's rainy season, we test whether differences in drought frequency between districts exceed those expected by chance, characterise drought events and their spatial coherence, and assess trends in seasonal SPI at district and grid-

cell scales. We also examine associations between drought variability and ENSO and the IOD, and provide recommendations for characterising drought exposure in subsequent CLIMATCH analyses of drought and the use of diabetes and hypertension services.

2 Data and methods

2.1 Study area

The study covers eight districts of mainland Tanzania: Bahi and Chamwino (Dodoma region), Meatu (Simiyu), Same (Kilimanjaro), Biharamulo (Kagera), Kibondo and Uvinza (Kigoma) and Nkasi (Rukwa) (Table 1; Fig. 1). They were purposively selected within CLIMATCH to represent unimodal and bimodal rainfall regimes and contrasting historical drought experience. Bahi, Chamwino, Meatu and Same had been classified as drought-prone, on the basis of past crop failure and food insecurity and advice from the Tanzania Meteorological Authority (TMA), and the other four as non-drought-prone (CLIMATCH, unpublished data). Mean annual rainfall ranges from about 640 mm in the semi-arid central districts of Bahi and Chamwino to about 1,150 mm in Kibondo and Uvinza (twelve times the monthly means in Table 2). The seasonal cycle (Fig. 2) shows a single November-April season in Bahi, Chamwino and Nkasi. Kibondo and Uvinza also receive most rain between November and April, with a weak dip in January-February and transitional rains in October and May, and were treated as unimodal. Biharamulo, Meatu and Same show distinct MAM and OND peaks and were treated as bimodal.

Table 1 Study districts, rainfall regimes and season-matched drought indices

District	Region	CLIMATCH group	Season(s) analysed	Season-matched index (end month)
Unimodal districts (November-April season)				
Bahi	Dodoma	Drought-prone	Nov-Apr	SPI-6 (April)
Chamwino	Dodoma	Drought-prone	Nov-Apr	SPI-6 (April)
Kibondo	Kigoma	Non-drought-prone	Nov-Apr	SPI-6 (April)
Nkasi	Rukwa	Non-drought-prone	Nov-Apr	SPI-6 (April)
Uvinza	Kigoma	Non-drought-prone	Nov-Apr	SPI-6 (April)
Bimodal districts (MAM and OND seasons)				
Biharamulo	Kagera	Non-drought-prone	MAM; OND	SPI-3 (May; December)
Meatu	Simiyu	Drought-prone	MAM; OND	SPI-3 (May; December)
Same	Kilimanjaro	Drought-prone	MAM; OND	SPI-3 (May; December)

Nov-Apr: November-April; MAM: March-May; OND: October-December. CLIMATCH groups were defined from historical crop failure and food insecurity, and TMA advice (CLIMATCH, unpublished data).

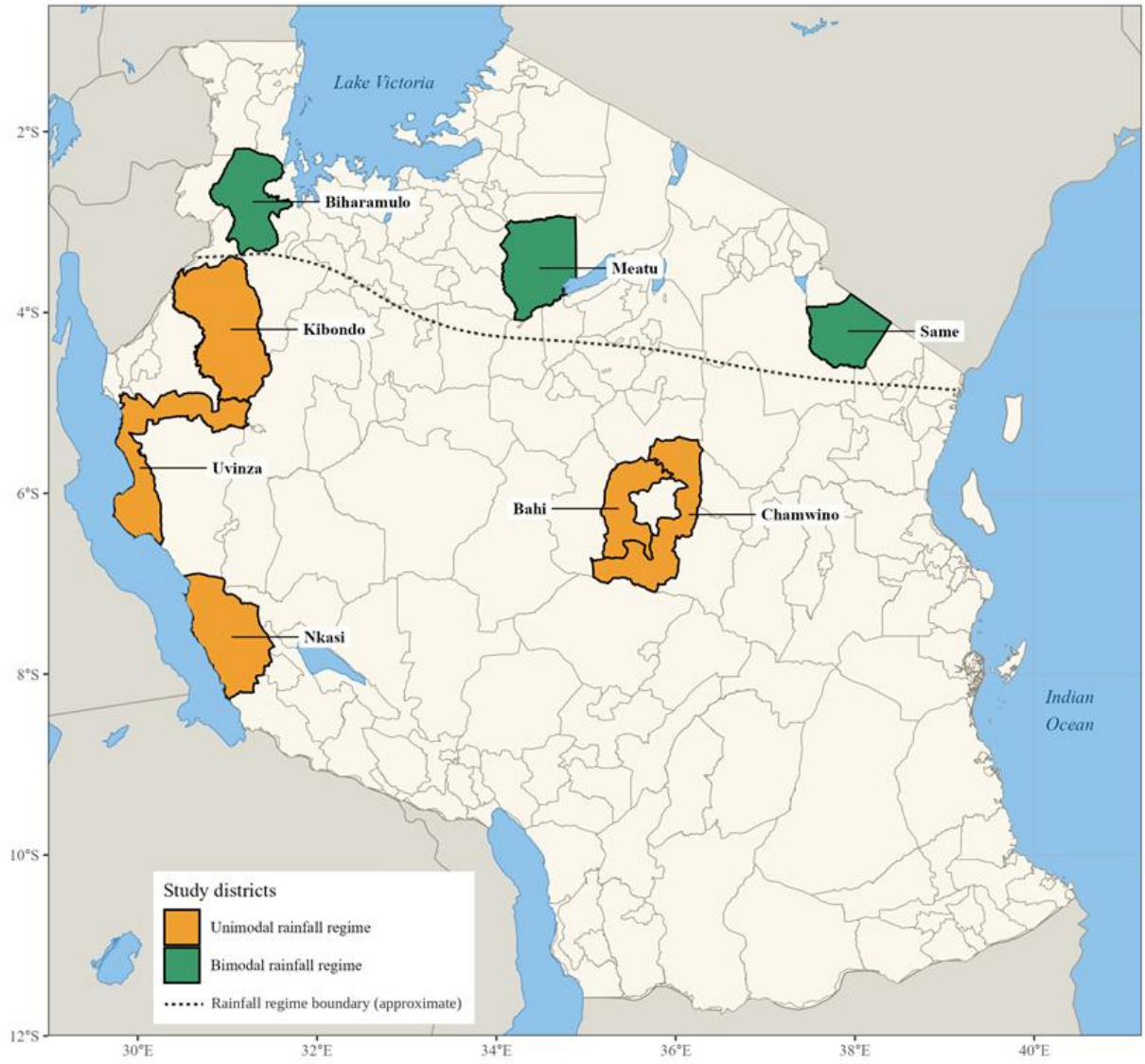


Fig. 1 Location of the eight study districts in mainland Tanzania

2.2 Data sources

Daily precipitation data for 1 January 1995 to 31 December 2024 were obtained from version 2.0 of the Climate Hazards Group InfraRed Precipitation with Station data (CHIRPS), a quasi-global gridded dataset at 0.05° spatial resolution developed by the Climate Hazards Center at the University of California, Santa Barbara. CHIRPS combines satellite-based infrared precipitation estimates with rain-gauge observations (Funk et al. 2015).

District-mean daily series were extracted by TMA and aggregated to monthly totals. As a check, we recalculated monthly district averages directly from the gridded CHIRPS data; the two series agreed closely (correlation ≥ 0.999; mean annual rainfall differing by at most 0.6%).

The suitability of CHIRPS for rainfall estimation in East Africa has been evaluated against rain-gauge observations. Dinku et al. (2018) assessed CHIRPS using observations from approximately 1,200 rain-gauge stations across the region, including Tanzania. For Tanzania, monthly CHIRPS estimates achieved a correlation coefficient of 0.86, an efficiency coefficient of 0.73, and a mean absolute error (MAE) of 29.6 mm. At the monthly timescale, CHIRPS performed better than the African Rainfall Climatology version 2 (ARC2) and the Tropical Applications of Meteorology using Satellite Data and ground-based observations version 3 (TAMSAT3) across these evaluation metrics. However, performance varied spatially and was weaker in coastal and mountainous areas. These findings support the use of CHIRPS to characterise historical rainfall variability in Tanzania, while highlighting the need to account for potential spatial uncertainties when interpreting drought patterns.

ENSO and the IOD were represented by their standard indices: the Oceanic Niño Index (ONI) of the United States National Oceanic and Atmospheric Administration (NOAA) Climate Prediction Center, based on Niño-3.4 sea surface temperature (SST) anomalies from the Extended Reconstructed Sea Surface Temperature dataset, version 6 (ERSSTv6; Huang et al. 2025), and the Dipole Mode Index (DMI; Saji et al. 1999), the west-east SST anomaly difference across the tropical Indian Ocean, computed from the Hadley Centre Sea Ice and Sea Surface Temperature dataset, version 1.1 (HadISST1.1; Rayner et al. 2003). Both indices are widely used in studies of East African rainfall (Black et al. 2003; Behera et al. 2005; Makula et al. 2025) and correspond to drivers that TMA uses to explain rainfall variability in Tanzania (TMA 2025). Because NOAA

adopted the Relative ONI (RONI), which subtracts the mean tropical SST anomaly, as its official ENSO index in February 2026 (NOAA NWS 2026), the ENSO correlation and partial correlation analyses were repeated with the RONI; the ONI was retained as the primary index for comparability with earlier East African studies. The DMI was linearly detrended to remove a significant warming trend of 0.09 °C per decade (1981-2024; Mann-Kendall test on annual means, $p < 0.001$), and the sensitivity of the results to this choice was tested.

2.3 SPI and season matching

SPI was computed in R at 1-, 3-, 6- and 12-month accumulation periods following Equations 1-8, which use the same gamma fitting as the SPEI package (Beguería et al. 2014). For an accumulation period of k months, the accumulated precipitation ending in month t is

$$X_t^{(k)} = \sum_{j=0}^{k-1} P_{t-j} \tag{1}$$

where P_t is the total precipitation in month t. For each calendar month, the non-zero accumulated totals were fitted with a two-parameter gamma distribution with probability density function

$$g(x) = \frac{x^{\alpha-1}\mathrm{e}^{-x/\beta}}{\beta^{\alpha}\,\Gamma(\alpha)}, \quad x > 0 \tag{2}$$

where $\alpha > 0$ is the shape parameter, $\beta > 0$ is the scale parameter and $\Gamma(\alpha)$ is the gamma function (McKee et al. 1993). The parameters were estimated by unbiased probability-weighted moments (Hosking 1990). With the n non-zero accumulated totals for a calendar month sorted in ascending order, $x_{(1)} \le x_{(2)} \le \cdots \le x_{(n)}$, the first two probability-weighted moments are

$$b_0 = \frac{1}{n}\sum_{i=1}^{n} x_{(i)}\,, \qquad b_1 = \frac{1}{n}\sum_{i=1}^{n} \frac{i-1}{n-1}\, x_{(i)} \tag{3}$$

172 from which the first two L-moments and the L-coefficient of variation are

173 $$\lambda_1 = b_0, \qquad \lambda_2 = 2b_1 - b_0, \qquad \tau = \frac{\lambda_2}{\lambda_1} \tag{4}$$

174 The shape parameter was obtained from τ using the rational approximation of Hosking (1990):

175 $$\alpha = \begin{cases} \dfrac{1 - 0.3080\, z}{z - 0.05812\, z^2 + 0.01765\, z^3}, & z = \pi\tau^2, \quad 0 < \tau < 0.5 \\ \dfrac{0.7213\, z - 0.5947\, z^2}{1 - 2.1817\, z + 1.2113\, z^2}, & z = 1 - \tau, \qquad 0.5 \le \tau < 1 \end{cases} \tag{5}$$

176 and the scale parameter as

177 $$\beta = \frac{\lambda_1}{\alpha} \tag{6}$$

178 Because accumulated precipitation can be zero, particularly at short accumulation periods in the
179 semi-arid districts, the cumulative probability was computed as a mixed distribution

180 $$H(x) = q + (1 - q)\, G(x) \tag{7}$$

181 where q is the proportion of zero totals for the calendar month and $G(x)$ is the cumulative
182 distribution function of the fitted gamma distribution (Guttman 1999). Monthly totals below 0.1
183 mm, trace amounts that result from summing near-zero daily CHIRPS estimates, were treated as
184 zero. Calendar months with fewer than four non-zero totals, which occurred only in the dry season
185 at SPI-1 and SPI-3, could not be fitted and were left missing. The cumulative probability was then
186 transformed to the standard normal distribution:

187 $$\mathrm{SPI} = \Phi^{-1}[H(x)] \tag{8}$$

where Φ^{-1} is the inverse of the standard normal cumulative distribution function, so that SPI has a mean of zero and a standard deviation of one. The full 1995-2024 record served as the reference period. Normality of the resulting SPI was checked month by month with the Shapiro-Wilk test (Stagge et al. 2015).

Because an SPI value integrates precipitation over the preceding k months, the accumulation period must equal the season of interest. For the unimodal districts we used SPI-6 ending in April, which integrates November-April. For the bimodal districts we used SPI-3 ending in May (MAM) and SPI-3 ending in December (OND). SPI-6 was not used for the bimodal seasons because a 6-month window extends beyond each 3-month season. Specifically, SPI-6 ending in May covers December-May rather than March-May, and SPI-6 ending in December covers July-December rather than October-December. Each district therefore contributed one (unimodal) or two (bimodal) seasonal series of 29-30 values, giving eleven district-season series in total. Drought classes followed the classification of Svoboda et al. (2012): moderate (-1.49 to -1.0), severe (-1.99 to -1.5) and extreme (≤ -2.0).

The accumulation period was therefore fixed in advance by a single climatological rule, not selected from the results: for every seasonal analysis (trends, links with ENSO and the IOD, and grid-cell maps), the SPI timescale equals the length of the rainy season being assessed. In particular, no timescale was chosen by its agreement with the CLIMATCH drought-prone classification, because that classification combined drought impacts, such as crop failure and food security, with meteorological advice from TMA and is therefore not a purely meteorological measure of hazard.

SPI-1 was not used for inference because no rainy season in the study area is one month long, and SPI-12 was not used for seasonal inference because in the bimodal districts it combines the MAM

and OND seasons. Analyses that follow SPI month by month and compare districts directly (drought events, return periods, regional coverage, spatial coherence and lagged correlations) require a single timescale common to all districts; for these we used SPI-6, which reflects seasonal to medium-term precipitation anomalies (Svoboda et al. 2012). Because this choice is conventional rather than climatologically determined, the event analysis was repeated with SPI-3 and SPI-12, with similar results (Table S1 in Online Resource 1).

2.4 Comparing drought frequency between districts

Because SPI is standardised at each location, the probability that a seasonal value falls at or below -1.5 is $\Phi(-1.5) = 0.067$ in every district, irrespective of its aridity. For each district and timescale, we compared the observed number of severe or extreme seasons with the 95% range of a binomial distribution with this probability, and repeated the comparison for moderate-or-worse seasons (SPI $\leq$ -1.0; probability 0.159). Whether counts differed between districts more than expected by chance was tested with a χ^2 statistic whose null distribution was obtained by randomly permuting events across all district-seasons (20,000 permutations).

2.5 Trend detection and robustness to the analysis period

We tested each seasonal SPI series, and the corresponding seasonal rainfall totals, for a consistent upward or downward trend with the Mann-Kendall test (Mann 1945; Kendall 1975), and estimated the rate of change with Sen's slope (Sen 1968). Because this test can give false positives when values in consecutive years are correlated, we also applied the correction of Hamed and Rao (1998); because it made the trends more, not less, significant, the uncorrected and therefore more conservative *p*-values are reported. The Pettitt (1979) test was used to identify the year of any abrupt shift, and the innovative trend analysis of Şen (2012), which compares the sorted values of the first and second halves of the record, was used to examine whether the change affected dry and

wet seasons alike. Because eleven series were tested, p-values were adjusted for multiple testing with the false discovery rate (FDR) of Benjamini and Hochberg (1995). Finally, to check whether the trends depended on the choice of years, we repeated the Mann-Kendall test and Sen's slope after moving the start year from 1995 to 2005 (keeping 2024 as the end) and after moving the end year from 2015 to 2024 (keeping 1995 as the start).

2.6 Drought events and return periods

Drought events were identified from monthly SPI-3, SPI-6 and SPI-12 using run theory (Yevjevich 1967): following McKee et al. (1993), an event is a run of consecutive months with SPI < 0 in which SPI reaches -1.0 or lower at least once. For each event we recorded the onset, duration D (months), severity S (sum of |SPI| over the event), intensity (S/D) and peak (minimum SPI). Event statistics were compared between the two halves of the record, 1995-2009 and 2010-2024, with each event assigned to the period of its onset month.

Drought duration and severity are closely linked, because longer droughts tend to be more severe, so their return periods were estimated jointly rather than separately. For SPI-6 events, we modelled the dependence between duration (D) and severity (S) with a copula, a function that links two separately fitted distributions (Shiau 2006). First, the distributions of D and S were fitted to each district's events, choosing among the exponential, gamma, lognormal and Weibull distributions by the Akaike information criterion (AIC) and checking the fit with Kolmogorov-Smirnov tests. Because each district had only 10-17 events, too few to estimate the dependence reliably, the strength of the link between D and S was estimated from the events of all districts combined, after ranking the events within each district. Four common copulas (Gaussian, Gumbel, Clayton and Frank) were compared, and the one with the lowest AIC was used. The joint return period, the

average time between events that are at least as long as d months and at least as severe as s, was then calculated as

$$T_{\mathrm{AND}} = \frac{\mu}{1 - F_D(d) - F_S(s) + C\big(F_D(d),\, F_S(s)\big)} \tag{9}$$

where μ is the mean inter-arrival time of drought events (the length of the SPI-6 record, June 1995-December 2024, divided by the number of events), F_D and F_S are the fitted distributions of duration and severity, and C is the copula. Uncertainty in the return periods was estimated by resampling each district's events 500 times (bootstrap), with the copula held fixed, so the intervals do not include uncertainty in the dependence structure.

2.7 Spatial coherence of drought

To examine whether districts experienced drought at the same time, we correlated the monthly SPI-6 series of every pair of districts (Pearson r) and grouped districts with similar drought histories by hierarchical clustering (average linkage, using 1 − r as the distance between districts). The number of districts with SPI-6 ≤ -1.0 in each month was used as a simple index of how widespread drought was across the study area.

2.8 Grid-cell analysis within districts

District means can hide differences within a district, so SPI was also calculated separately for every 0.05° CHIRPS grid cell whose centre fell inside a study district, using each cell's own monthly CHIRPS v2.0 rainfall for 1995-2024 and the same gamma fitting as for the district series (Equations 1-8), computed with the SPEI package. District boundaries were taken from the national administrative shapefile and transformed to the World Geodetic System 1984 (WGS84) to match CHIRPS. The eight districts contained 2,311 grid cells. From each cell's monthly SPI,

one value per year was extracted at the end of each season, using the same season matching as for the district series: SPI-6 ending in April for the unimodal districts, and SPI-3 ending in May (MAM) and December (OND), analysed separately, for the bimodal districts. The 1,569 cells in unimodal districts contributed one series each and the 742 cells in bimodal districts two each, giving 3,053 cell-season series.

For each series, the trend was tested with the Mann-Kendall test and its magnitude estimated with Sen's slope, and the association with the season-matched, linearly detrended DMI was measured with the Pearson correlation. Using one value per year avoided the overlap between consecutive monthly accumulations. As for the district series, applying the Hamed and Rao (1998) correction would have made more trends significant, so the uncorrected and therefore more conservative *p*-values are reported. Because thousands of tests were performed, the Benjamini-Hochberg false discovery rate (FDR) was applied separately to the trend tests and the DMI correlations across all 3,053 cell-season series (Wilks 2016). Results with an FDR-adjusted $q < 0.05$ were considered statistically significant.

2.9 Links with ENSO and the IOD

Each seasonal SPI value was paired with the ENSO and IOD index values for the months relevant to that season. For OND, we used the OND ONI and the September-November DMI of the same year. For November-April, we used the November-January ONI and the September-November DMI at the start of the season, because IOD events usually peak in September-November and decay by January (Saji et al. 1999); this examined whether the IOD state at the onset of the season was associated with the seasonal outcome. For MAM, we used the MAM ONI and the March-May DMI. The association between SPI and each index was measured with Pearson correlations, and Spearman rank correlations were calculated, without significance testing, as a check less

influenced by extreme years. Because ONI and DMI were correlated in OND and November-April (r = 0.66-0.68), although only weakly in MAM (r = 0.18), partial correlations were also calculated to assess the association between SPI and each index while accounting for the other.

Seasons were classified into threshold-defined phases from their own index values: El Niño (ONI ≥ 0.5 °C), La Niña (ONI ≤ -0.5 °C), positive IOD (DMI ≥ 0.4 °C) and negative IOD (DMI ≤ -0.4 °C), with all other seasons treated as neutral. SPI in each phase was compared with SPI in neutral seasons using Mann-Whitney tests. IOD phases were compared only for OND and November-April, because the March-May DMI did not reach ±0.4 °C in any year. To assess whether the increase in SPI over time was associated with the two modes, SPI was regressed first on year alone and then on year, ONI and DMI together; a smaller estimated coefficient for year in the second model was interpreted as a statistical attenuation of the trend, not as proof of cause. The p-values were adjusted with the Benjamini-Hochberg FDR across the district-season series, separately for the Pearson correlations, the partial correlations, each of the four phase comparisons and the year coefficient, and results with an FDR-adjusted $q < 0.05$ were considered significant. Finally, lagged correlations between monthly SPI-6 and the indices 0-6 months earlier were calculated as an exploratory, descriptive measure of the timing of the association, without significance testing, because consecutive monthly SPI-6 values overlap.

2.10 Data analysis

All analyses were carried out in R 4.5.1. SPI was computed from Equations 1-8 and checked against the SPEI package, version 1.8.1 (Beguería et al. 2014). The Mann-Kendall, Sen's slope and Pettitt tests used the trend package, version 1.1.6 (Pohlert 2023). Furthermore, the Hamed-Rao correction and the innovative trend analysis were coded directly. Copulas were fitted with the copula package, version 1.1.7 (Yan 2007), and the duration and severity distributions with MASS,

version 7.3-65 (Venables and Ripley 2002). Gridded and vector data were processed with terra, version 1.8-54 (Hijmans 2025), and sf, version 1.1.1 (Pebesma 2018), and figures were drawn with ggplot2, version 3.5.2 (Wickham 2016).

3 Results

3.1 Data completeness and rainfall climatology

The rainfall dataset comprised 87,664 daily observations, 10,958 for each district, from 1 January 1995 to 31 December 2024, which aggregated to 2,880 district-months (360 per district). No missing, invalid or duplicated dates, missing or negative rainfall values, or records outside the study period were found at the daily level, and no missing, negative, incomplete or duplicated months were found after aggregation. The dataset therefore had complete temporal coverage and passed all data-quality checks, and was retained for the subsequent analyses.

Mean monthly rainfall ranged from 53.6 mm in Chamwino to 96.4 mm in Kibondo (Fig. 2a; Table 2). The four CLIMATCH drought-prone districts (Bahi, Chamwino, Meatu, and Same) had lower mean monthly rainfall (53.6-59.5 mm) than the four non-drought-prone districts (Biharamulo, Kibondo, Nkasi, and Uvinza; 88.1-96.4 mm). Monthly rainfall was strongly right-skewed in the semi-arid central districts, where medians (6.0 mm in Bahi and 9.5 mm in Chamwino) were far below means and 61-67% of days were rainless. Nkasi showed a similar contrast (median 44.1 mm against a mean of 88.1 mm), reflecting its long dry season, whereas in Uvinza, Kibondo, and Biharamulo means and medians were similar. Monthly variability was greatest in Nkasi (SD = 94.8 mm) and smallest in Same (58.6 mm).

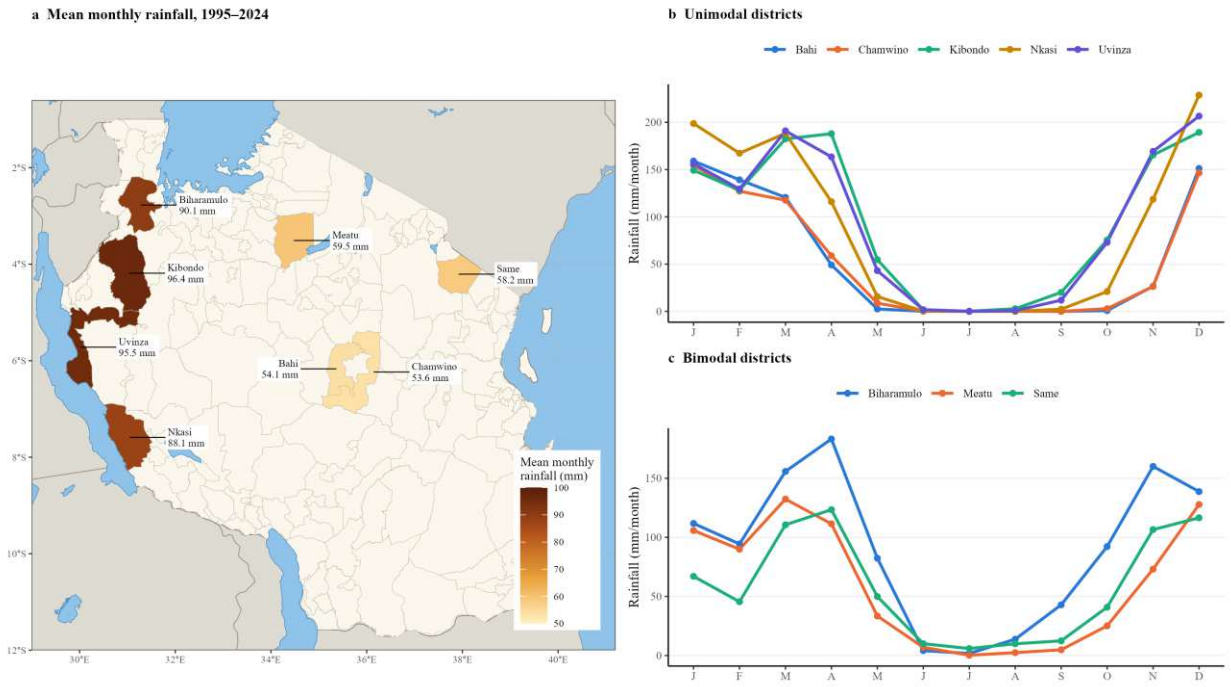


Fig. 2 Rainfall in the study districts, 1995-2024. (a) Mean monthly rainfall by district. (b, c) Mean monthly rainfall climatology for the unimodal and bimodal districts

Table 2 Descriptive statistics of monthly rainfall in the study districts, 1995-2024

District	CLIMATCH group	Mean (mm/month)	Median (mm/month)	SD (mm/month)	Rainless days (%)
Unimodal districts (November-April season)					
Bahi	Drought-prone	54.1	6.0	77.6	67
Chamwino	Drought-prone	53.6	9.5	72.7	61
Kibondo	Non-drought-prone	96.4	91.4	84.8	41
Nkasi	Non-drought-prone	88.1	44.1	94.8	43
Uvinza	Non-drought-prone	95.5	92.9	86.6	38
Bimodal districts (MAM and OND seasons)					
Biharamulo	Non-drought-prone	90.1	87.9	70.0	38
Meatu	Drought-prone	59.5	39.8	59.0	50
Same	Drought-prone	58.2	39.0	58.6	60

Statistics are computed over 360 monthly totals per district. Rainless days: percentage of daily records with zero rainfall. SD: standard deviation.

The seasonal cycles confirmed the regime classification (Fig. 2b, c). Bahi, Chamwino, and Nkasi had a single November-April season with almost no rain from June to September. Kibondo and Uvinza also received most rain between November and April but with a more pronounced dip in January-February and transitional rains in October and May. Biharamulo, Meatu, and Same had distinct MAM and OND peaks. In all districts, rainfall was lowest in June-September.

Seasonal rainfall totals differed substantially between districts and rainfall regimes (Table 3; Fig. 3). Among the unimodal districts, mean November-April rainfall was about 630-644 mm in Bahi and Chamwino, compared with 1,000-1,017 mm in Kibondo, Nkasi and Uvinza. Among the bimodal districts, Biharamulo received the most rain in both MAM (421 mm) and OND (391 mm), compared with 277 and 226 mm in Meatu and 284 and 264 mm in Same. OND rainfall was more variable than MAM rainfall in all three bimodal districts, particularly in Same (SD = 132 mm in OND against 87 mm in MAM). Seasons with rainfall above the upper whisker of the box plots occurred in Bahi (2019/20 and 2021/22), Chamwino (2019/20), Nkasi and Uvinza (2023/24), Meatu MAM (2006, 2013 and 2018), Same MAM (2018 and 2020) and Same OND (2019); nine of these eleven seasons occurred from 2018 onwards. These differences in seasonal amount, timing and variability are why drought was characterised with season-matched SPI rather than with rainfall totals alone.

Table 3 Seasonal rainfall in the study districts, 1995-2024

District	CLIMATCH group	Season	Complete seasons	Mean (mm)	Median (mm)	SD (mm)	Range (mm)
Unimodal districts (November-April season)							
Bahi	Drought-prone	Nov-Apr	29	644	597	184	377-1,118
Chamwino	Drought-prone	Nov-Apr	29	630	591	168	378-1,094
Kibondo	Non-drought-prone	Nov-Apr	29	1,000	965	171	814-1,436
Nkasi	Non-drought-prone	Nov-Apr	29	1,017	949	168	791-1,555
Uvinza	Non-drought-prone	Nov-Apr	29	1,016	991	158	844-1,511
Bimodal districts (MAM and OND seasons)							
Biharamulo	Non-drought-prone	MAM	30	421	410	74	274-619
	Non-drought-prone	OND	30	391	374	89	232-546
Meatu	Drought-prone	MAM	30	277	274	73	174-473
	Drought-prone	OND	30	226	235	89	74-426
Same	Drought-prone	MAM	30	284	261	87	175-557
	Drought-prone	OND	30	264	222	132	88-573

Complete seasons: November-April seasons require November-December of the preceding year, so the first season is 1995/96 (29 seasons); MAM and OND have 30 seasons. SD: standard deviation.

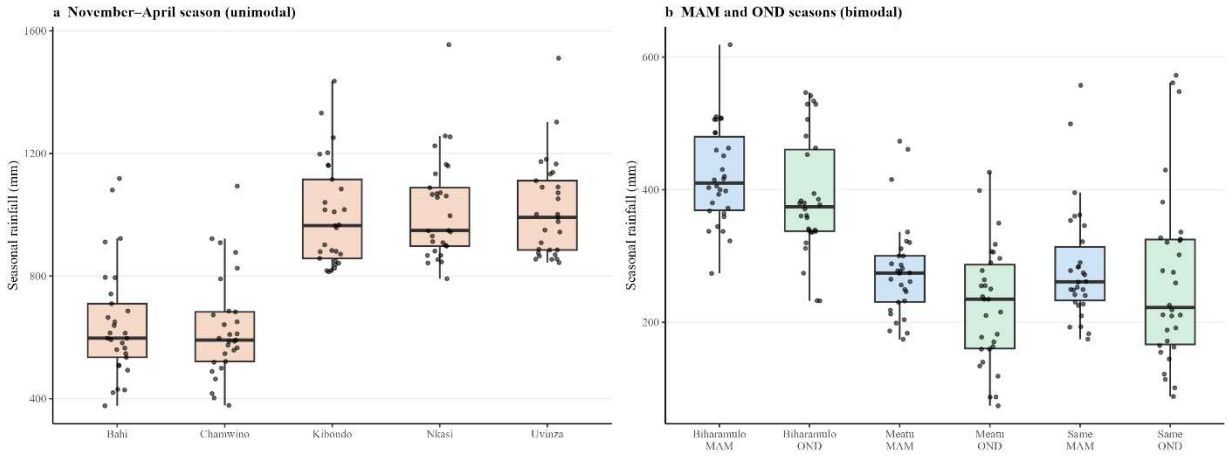


Fig. 3 Distribution of seasonal rainfall totals in the eight study districts, 1995-2024: (a) November-April rainfall in the five unimodal districts; (b) March-May (MAM) and October-December (OND) rainfall in the three bimodal districts. Boxes show the interquartile range and horizontal lines the median; whiskers extend to the most extreme seasons within 1.5 times the interquartile range; points show individual seasonal totals, and those beyond the whiskers are statistical outliers of each distribution

3.2 Normality of SPI

Departures from normality in SPI were concentrated in the dry months, particularly in the semi-arid districts. In Bahi and Chamwino, where 22-31% of monthly rainfall totals were below 0.1 mm, SPI-1 and SPI-3 showed statistically significant departures from normality (Shapiro-Wilk test, $p < 0.05$) in three to five of the twelve calendar months (Table S2 in Online Resource 1), predominantly between May and September (13 of 17 significant month-specific tests). By contrast, the season-matched SPI series used for inference showed limited evidence of departure from normality: seven of the eleven series had non-significant Shapiro-Wilk tests, and the remaining four (November-April SPI-6 in Kibondo, Nkasi and Uvinza, and MAM SPI-3 in Same) had unadjusted p-values of 0.013-0.046, none of which remained significant after false discovery rate adjustment ($q = 0.110$-0.126). SPI-12 in Same departed from normality in eight of the twelve calendar months, so results for this timescale and district should be interpreted with caution.

3.3 Between-district differences in drought frequency

At every timescale and in every district, the number of severe or extreme seasons fell within the 95% range expected by chance for a standardised index (Fig. S1 in Online Resource 1). The permutation test found no evidence that drought frequency differed between districts at SPI-1, SPI-3, SPI-6 or SPI-12 (Monte-Carlo $p = 0.81$, 0.84, 0.43 and 0.65; Table S3 in Online Resource 1), and the same held for moderate-or-worse seasons (SPI $\leq$ -1.0; Monte-Carlo $p = 0.92$-1.00). At SPI-6 and SPI-12, a larger share of seasons was severe or extreme in the CLIMATCH drought-prone than in the non-drought-prone districts (6.2% versus 2.7%), but this contrast lies within the range

expected by chance in every district and reverses at SPI-1 and SPI-3 (6.1% versus 7.3%, and 3.3% versus 4.7%). The analysis therefore provides no evidence that drought frequency differs between districts. Drought proneness in the CLIMATCH study reflects the consequences of rainfall deficits for crops and food security in drier environments, rather than a higher frequency of standardised deficits, and the two should be treated as different concepts.

3.4 Temporal changes and their sensitivity to the analysis period

Season-matched SPI showed positive estimated trends in all eleven district-season series, with Sen's slopes of 0.08-0.68 SPI units per decade, and estimated seasonal rainfall totals increased by 2-18% per decade (Table 4; Fig. 4). Mean SPI shifted from -0.39 to -0.18 in 1995-2009 to +0.17 to +0.37 in 2010-2024. After FDR adjustment, trends were significant in four series: Kibondo (q = 0.012), Meatu MAM (q = 0.012), Biharamulo OND (q = 0.027) and Uvinza (q = 0.028). Bahi, Chamwino and Same OND had trends with $p < 0.05$ that did not remain significant after adjustment, Nkasi, Biharamulo MAM and Meatu OND had weaker trends (p = 0.053-0.094; q = 0.073-0.103), and Same MAM showed no trend (τ = 0.05, q = 0.70). Pettitt change points fell in 2006-2018; the shifts in Kibondo (2018) and Meatu MAM (2006) were significant at the 5% level. Innovative trend analysis showed that the driest seasons became less dry in all eleven series: the driest third of seasons had SPI values 0.08-1.31 units higher in the second half of the record than in the first. In the unimodal districts the wettest seasons also became wetter (by 0.81-1.11 units), whereas in Meatu OND and Same OND the wettest seasons did not change (-0.13 and -0.09), so the change there consisted of fewer and milder dry seasons rather than wetter wet seasons.

Table 4 Trends in season-matched SPI and seasonal rainfall, 1995-2024

District	Season	Kendall τ	MK p	FDR q	Sen slope per decade	Pettitt year (p)	Rainfall change (%/decade)	Mean SPI 1995-2009	Mean SPI 2010-2024
Unimodal districts (November-April season)									
Bahi	Nov-Apr	0.27	0.045	0.070	0.46	2018 (0.08)	+12.0	-0.29	0.29
Chamwino	Nov-Apr	0.29	0.031	0.068	0.45	2018 (0.08)	+11.7	-0.28	0.28
Kibondo	Nov-Apr	0.40	0.002	0.012*	0.68	2018 (0.01)	+11.5	-0.39	0.37
Nkasi	Nov-Apr	0.26	0.053	0.073	0.52	2016 (0.19)	+7.8	-0.18	0.17
Uvinza	Nov-Apr	0.34	0.010	0.028*	0.62	2013 (0.10)	+9.2	-0.29	0.28
Bimodal districts (MAM and OND seasons)									
Biharamulo	MAM	0.23	0.080	0.098	0.42	2009 (0.18)	+7.1	-0.32	0.33
	OND	0.35	0.007	0.027*	0.45	2011 (0.13)	+10.1	-0.35	0.36
Meatu	MAM	0.40	0.002	0.012*	0.49	2006 (0.01)	+12.1	-0.37	0.37
	OND	0.22	0.094	0.103	0.47	2006 (0.42)	+17.6	-0.32	0.32
Same	MAM	0.05	0.695	0.695	0.08	2013 (0.88)	+2.2	-0.18	0.19
	OND	0.27	0.038	0.070	0.43	2011 (0.21)	+16.7	-0.24	0.27

MK: Mann-Kendall test (uncorrected; see Section 2.5). FDR q: Benjamini-Hochberg adjusted p across the eleven series (* $q < 0.05$). Pettitt year: first year of the new regime. Unimodal districts use SPI-6 ending in April; bimodal seasons use SPI-3 ending in May (MAM) or December (OND). Mann-Kendall results for seasonal rainfall totals are identical to those for SPI, because SPI preserves the ranking of seasonal totals.

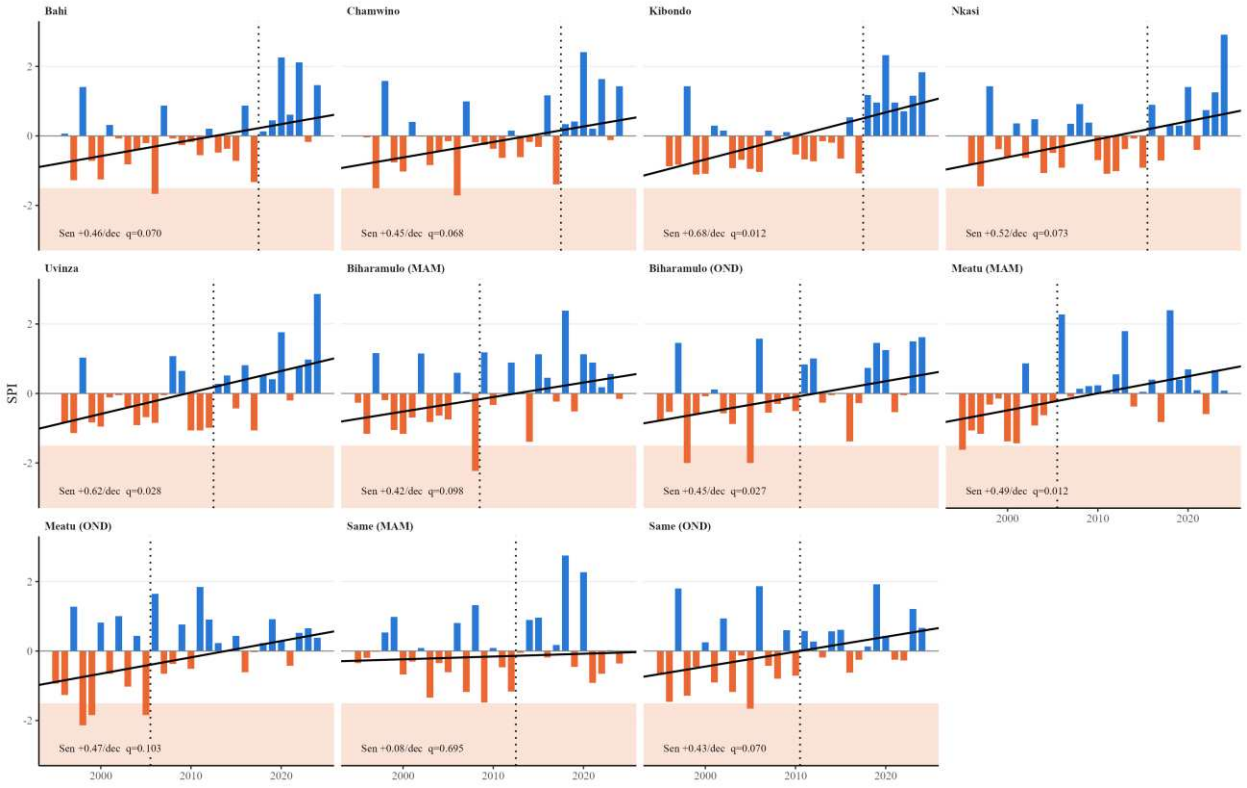


Fig. 4 Season-matched SPI, 1995-2024. Orange and blue bars show negative and positive seasonal SPI, the solid line Sen's slope and the dotted line the Pettitt change point; shading marks the severe/extreme range (SPI ≤ -1.5). Each panel gives Sen's slope per decade and the FDR-adjusted *q*-value

The trends were sensitive to the analysis period (Fig. 5). For the unimodal districts, Sen's slopes for windows ending in 2015-2019 were close to zero (-0.14 to +0.33 per decade) and none was significant; significance appeared only for end years in 2021-2024, and for Nkasi not at all. Kibondo and Uvinza remained significant for every start year between 1995 and 2005, whereas the Meatu MAM trend was significant for every end year but lost significance when the series started in 1999 or later, because it depends on the dry seasons of 1995-1998. No district-season was robust to changes in both the start and the end of the window. The wetting signal is therefore consistent in direction, but its strength and significance depend on the period analysed and are concentrated in the last five to six years of the record.

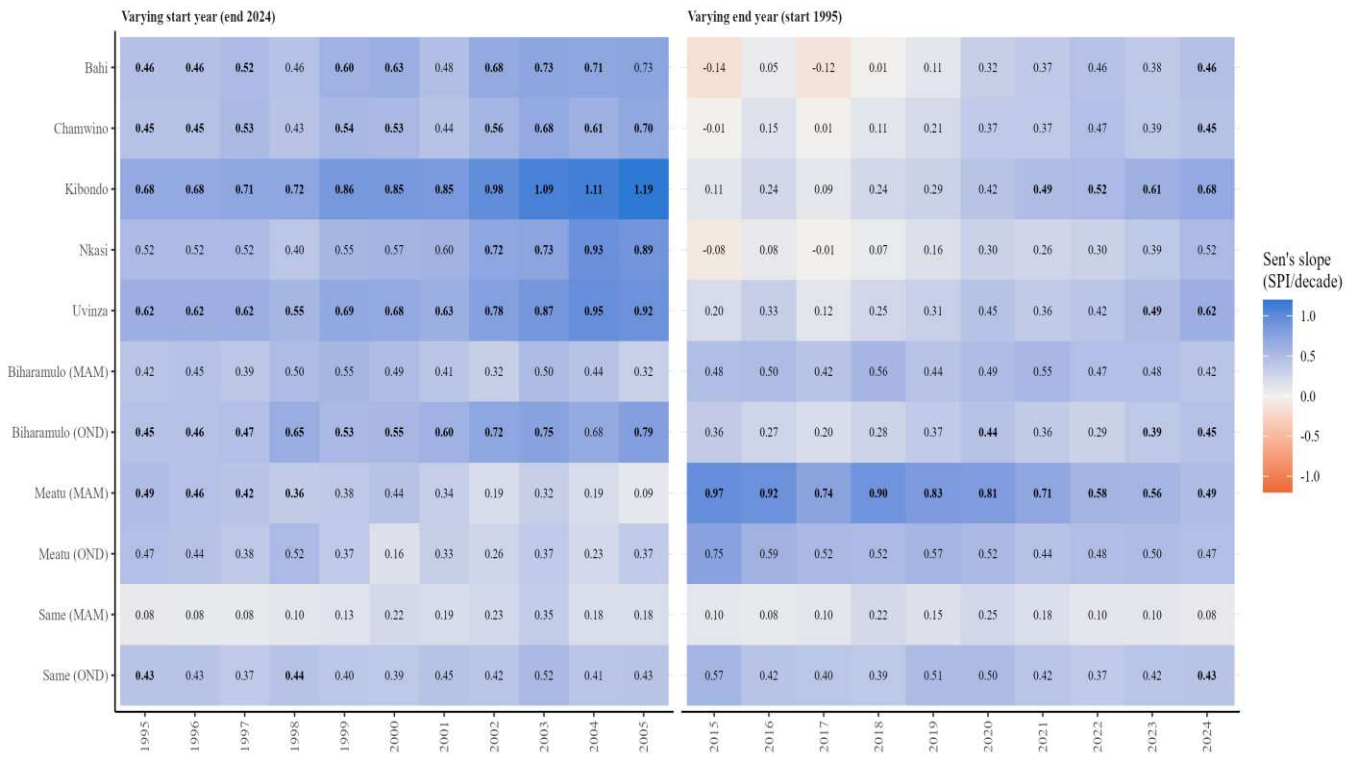


Fig. 5 Sensitivity of Sen's slope (SPI per decade) to the start year (left; end 2024) and end year (right; start 1995) of the analysis window. Bold values have Mann-Kendall $p < 0.05$ before FDR adjustment

3.5 Drought events and their recent decline

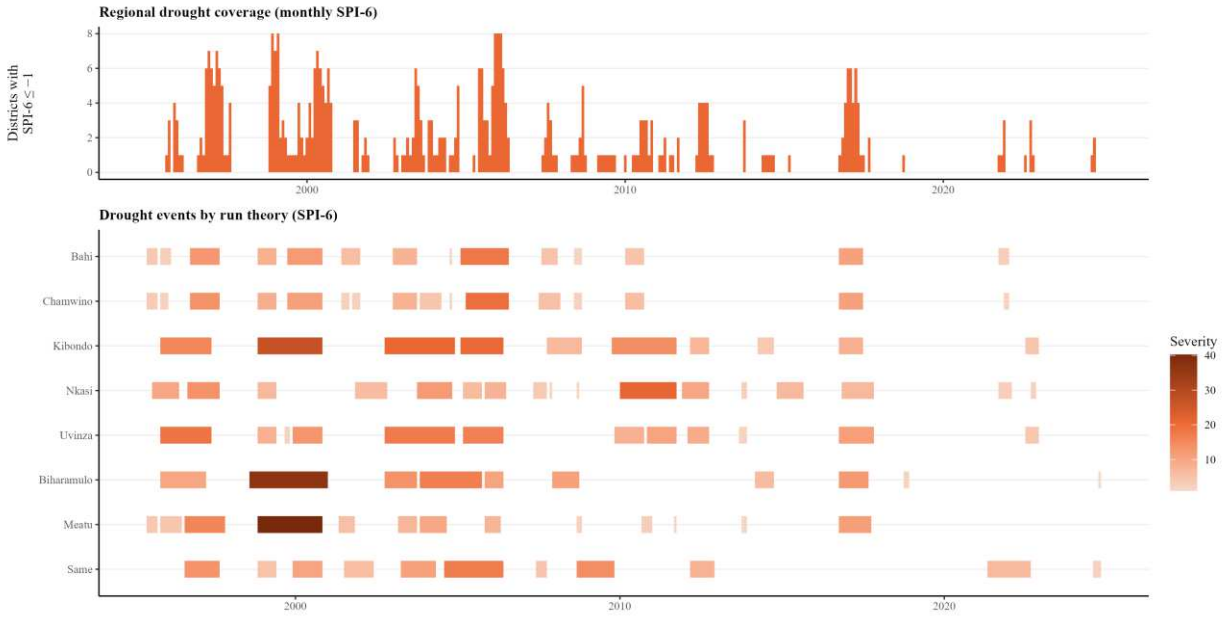
Run theory identified 103 SPI-6 drought events across the eight districts, 10-17 per district, with a mean duration of 9.4 months (Table 5). The longest and most severe events occurred in the western and lake-zone districts: the 1998-2000 drought lasted 24-29 months in Kibondo, Biharamulo and Meatu, with severities of 26.8, 36.6 and 40.2, respectively. The 2005-2006 drought was the most severe event in Bahi and Chamwino and affected all eight districts simultaneously (Fig. 6). Other widespread episodes occurred in 1996-1997, 2003-2004 and 2016-2017. Total SPI-6 drought months fell from 736 in 1995-2009 to 235 in 2010-2024 (-68%), with reductions of 71-80% in six districts but smaller declines in Uvinza (91 to 40 months) and Nkasi (76 to 62). The broad pattern was also observed at SPI-3 and SPI-12 (Table S1 in Online Resource 1): the same widespread episodes appear at all three timescales, and total drought months declined

447 at each of them (SPI-3: 623 to 305; SPI-12: 730 to 389), although the number and duration of
448 events differed between timescales. Nkasi was the only district in which drought months did not
449 decline at SPI-3 and SPI-12. As expected, shorter accumulation periods identified more and shorter
450 events (175 SPI-3 events; mean duration 5.3 months) and longer accumulations fewer and longer
451 ones (48 SPI-12 events; 23.3 months).

452 **Table 5 SPI-6 drought events identified by run theory, 1995-2024**

District	Events	Mean duration (months)	Max duration (months)	Mean severity	Mean intensity	Drought months 1995-2009 / 2010-2024	Most severe event: onset (duration; severity)
Unimodal districts (November-April season)							
Bahi	14	7.4	18	6.8	0.88	83 / 20	2005-02 (18 mo; S=17.9)
Chamwino	16	6.7	16	6.4	0.91	89 / 18	2005-04 (16 mo; S=19.4)
Kibondo	10	14.9	26	12.7	0.85	122 / 27	1998-11 (24 mo; S=26.8)
Nkasi	17	8.1	21	7.0	0.92	76 / 62	2010-01 (21 mo; S=21.2)
Uvinza	12	10.9	26	10.0	0.94	91 / 40	1995-11 (19 mo; S=18.4)
Bimodal districts (MAM and OND seasons)							
Biharamulo	10	11.9	29	11.9	1.02	98 / 21	1998-08 (29 mo; S=36.6)
Meatu	13	7.8	24	8.7	1.05	82 / 19	1998-11 (24 mo; S=40.2)
Same	11	11.2	22	8.9	0.82	95 / 28	2004-08 (22 mo; S=17.0)

453 An event is a run of months with SPI-6 < 0 that reaches ≤ -1.0. Severity *S* is the sum of |SPI| over the event;
454 intensity is *S* divided by duration.



455

456 **Fig. 6** Regional drought coverage and drought events in the eight study districts, 1995-2024. Top: number
457 of districts with SPI-6 ≤ -1.0 in each month. Bottom: drought events identified by run theory in each district,
458 defined as runs of months with SPI-6 below zero that reached -1.0 or lower; bars show the timing and
459 duration of each event, and colour shows its severity (the sum of |SPI-6| over the event)

460 Drought duration and severity were strongly dependent (pooled Kendall $\tau = 0.81$). The Gaussian
461 copula fitted best (AIC = -196, compared with -191 for Gumbel, -185 for Clayton and -180 for
462 Frank). Weibull distributions described duration in six districts (exponential in the other two), and
463 exponential, gamma, lognormal or Weibull distributions described severity, with all Kolmogorov-
464 Smirnov $p > 0.4$. An event lasting at least 6 months with severity of at least 6 recurs every 3.5-5.5
465 years, and an event of at least 9 months with severity of at least 10 every 5.3-11.4 years (Table 6).
466 The estimated return periods of the most severe observed events (36-172 years) are model-based
467 extrapolations far beyond the 30-year record; their very wide confidence intervals, with lower
468 bounds of 17-35 years, indicate only that such events are rare.

Table 6 Joint (AND) return periods of SPI-6 drought duration (*D*, months) and severity (*S*) from the Gaussian copula

District	Marginals (*D* / *S*)	T_{AND}: $D \geq 6$ and $S \geq 6$ (years, 95% CI)	T_{AND}: $D \geq 9$ and $S \geq 10$ (years, 95% CI)	T_{AND}: most severe observed event (years, lower 95% bound)
Unimodal districts (November-April season)				
Bahi	weibull / gamma	4.6 (3.1-8.8)	10.5 (6.0-50.8)	131 (>35)
Chamwino	weibull / lognormal	5.0 (3.2-11.9)	11.4 (6.6-64.0)	80 (>28)
Kibondo	weibull / gamma	3.7 (3.0-4.8)	5.3 (3.7-10.2)	54 (>24)
Nkasi	weibull / gamma	3.7 (2.6-6.5)	8.0 (4.9-21.7)	128 (>35)
Uvinza	weibull / weibull	3.5 (2.7-5.2)	5.7 (3.3-11.5)	36 (>17)
Bimodal districts (MAM and OND seasons)				
Biharamulo	exponential / exponential	5.3 (4.5-7.9)	7.5 (5.6-15.0)	69 (>26)
Meatu	exponential / lognormal	5.5 (4.0-10.6)	9.6 (5.7-48.8)	172 (>33)
Same	weibull / weibull	3.8 (3.0-5.4)	7.3 (4.1-24.1)	114 (>32)

Confidence intervals from 500 bootstrap resamples of each district's events. Upper bounds for the most severe events are not shown because they exceed the record length by orders of magnitude.

3.6 Spatial coherence

Monthly SPI-6 was positively correlated between all district pairs (r = 0.39-0.97; Fig. 7), indicating shared temporal variability in drought conditions across the study area, although its strength differed between pairs. Clustering separated a central semi-arid pair (Bahi-Chamwino, r = 0.97) that grouped loosely with Same, a western group (Kibondo-Uvinza, r = 0.87; Uvinza-Nkasi, r = 0.78), and the lake-zone districts of Biharamulo and Meatu, which joined the other districts last. These groupings cut across the CLIMATCH classification: non-drought-prone Kibondo was more strongly correlated with non-drought-prone Biharamulo (r = 0.77) than with any drought-prone district (r = 0.58-0.67), and drought-prone Meatu was more closely related to Biharamulo (r = 0.62) than to the central districts (r = 0.54-0.55).

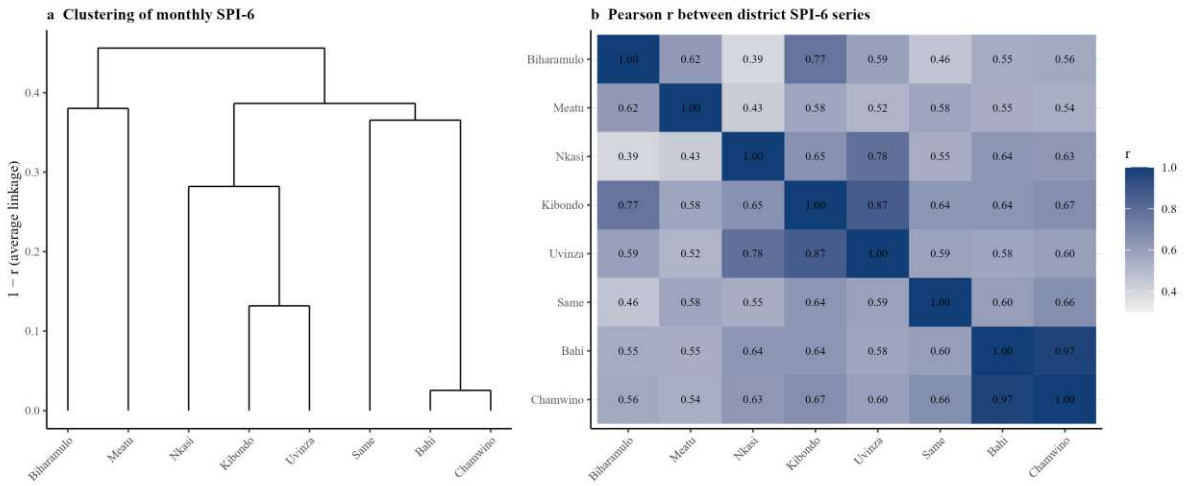


Fig. 7 Spatial coherence of monthly SPI-6 across the study districts: (a) hierarchical clustering (average linkage, distance $1 - r$); (b) Pearson correlation matrix

3.7 Within-district patterns of change

At the grid-cell scale, estimated SPI trends were positive in all cells in every district-season except Same MAM, where 70% of cells had positive and 30% weakly negative slopes, none of them significant (Fig. 8). No cell in any district-season showed a significant negative trend. The proportion of cells with significant positive trends after FDR correction was highest in Kibondo (91%), Uvinza (70%) and Meatu MAM (67%), smaller in Biharamulo OND (31%), Same OND (30%), Chamwino (28%), Nkasi (19%) and Biharamulo MAM (17%), and lowest in Bahi (10%) and Meatu OND (2%). Within districts, trends were strongest in eastern Kibondo, the northern arm and the southern block along Lake Tanganyika in Uvinza, eastern Meatu and southern Same, and weakest in the western Biharamulo and in central Nkasi. Cell-level slopes ranged from 0.13 to 0.79 SPI units per decade in the OND and November-April seasons, similar to the district-mean values in Table 4. The grid-cell analysis therefore supports the positive direction of the district-level trends, while showing that their strength and statistical significance varied substantially within districts.

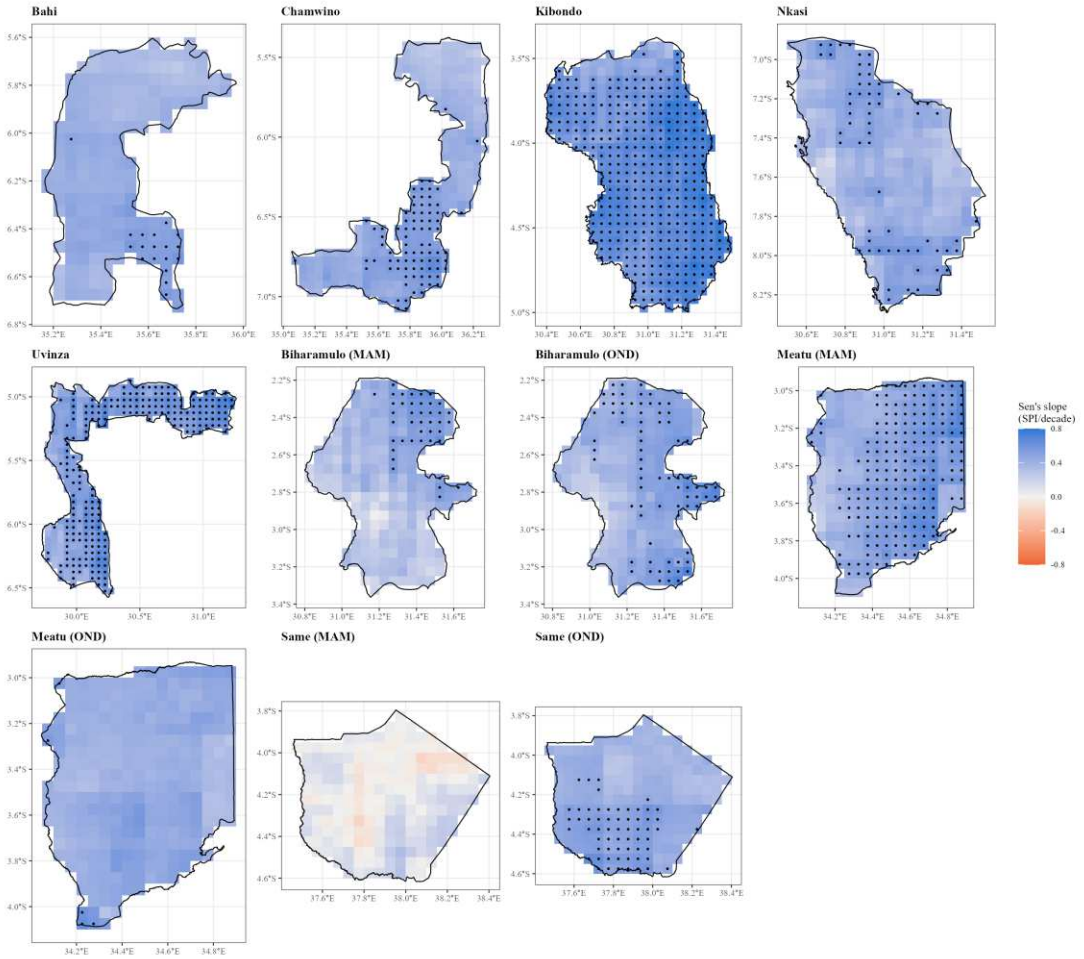


Fig. 8 Grid-cell Sen's slope of season-matched SPI (SPI units per decade), 1995-2024. Black dots mark cells with a significant positive Mann-Kendall trend after Benjamini-Hochberg false discovery rate correction across all 3,053 cell-season series. Unimodal districts use SPI-6 ending in April; bimodal districts use SPI-3 ending in May (MAM) and December (OND), analysed separately

3.8 Links between seasonal drought and ENSO and the IOD

For the OND and November-April seasons, SPI was strongly and positively correlated with the DMI in all eight series (r = 0.59-0.81, all $q < 0.01$) and more weakly with the ONI (r = 0.37-0.63; significant after FDR adjustment in five of eight) (Table 7; Fig. 9a). Controlling for ENSO left the DMI association almost unchanged (partial r = 0.44-0.67, all $q < 0.05$), whereas the partial correlation of SPI with ONI controlling for the DMI was close to zero (-0.07 to 0.19, none significant). Together the two modes explained 35-66% of interannual SPI variance, the most in

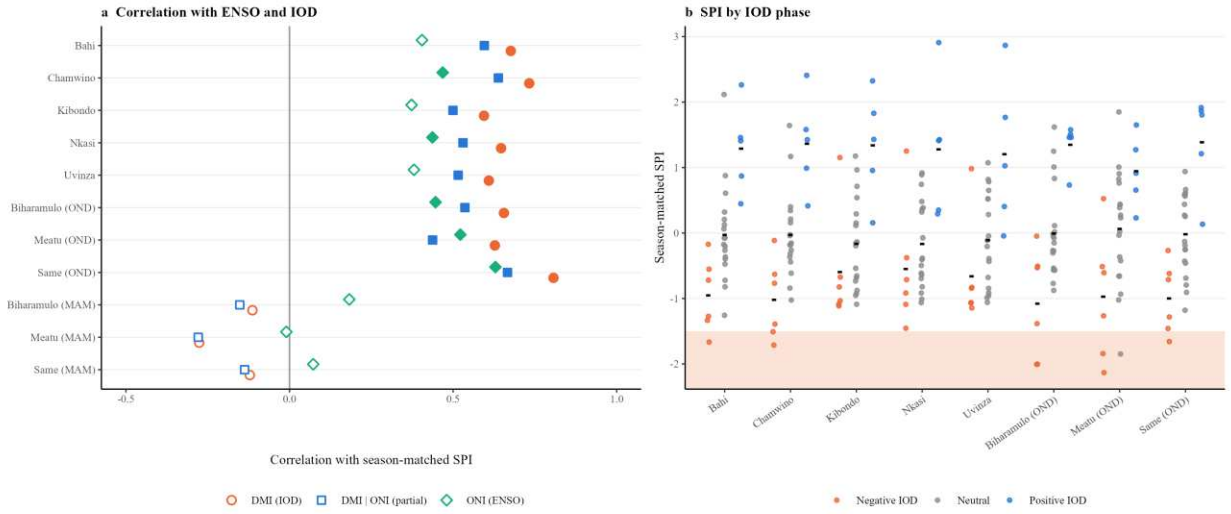
Same OND (66%) and Chamwino (54%). The DMI led monthly SPI-6 by 4-5 months, with peak lagged correlations of 0.31-0.49. MAM SPI showed no significant relationship with either index ($|r| \leq 0.28$).

Composites confirmed the asymmetric role of the IOD (Fig. 9b). Mean SPI in positive IOD seasons (1997, 2006, 2018, 2019 and 2023) was +0.94 to +1.39, and in negative IOD seasons (1996, 1998, 2005, 2010, 2016 and 2022) -0.55 to -1.08; the differences from neutral seasons remained significant after FDR adjustment ($q < 0.05$) in all eight series for positive IOD and in three for negative IOD (Bahi, Chamwino and Same OND). By contrast, SPI in El Niño and La Niña seasons did not differ significantly from neutral seasons in any series after FDR adjustment. All nine severe or extreme OND and November-April seasons occurred under negative (eight) or neutral (one) IOD conditions and under La Niña (eight) or neutral (one) ENSO; none occurred in a positive IOD or El Niño season. At the monthly scale, four or more districts were simultaneously in drought in only 3% of El Niño months, compared with 15-16% of La Niña and neutral months.

Table 7 Relationships between season-matched SPI and ENSO (ONI) and IOD (DMI), and the year effect with and without the modes

District	Season	*r* ONI	*r* DMI	Partial *r* DMI | ONI	Partial *r* ONI | DMI	R^2 (ONI + DMI)	Year effect alone (SPI/decade, p)	Year effect with ONI + DMI (SPI/decade, p)
Unimodal districts (November-April season)								
Bahi	Nov-Apr	0.40	0.68**	0.60**	-0.07	0.46	0.48 (0.023)	0.36 (0.028)
Chamwino	Nov-Apr	0.47*	0.73**	0.64**	-0.03	0.54	0.46 (0.030)	0.33 (0.033)
Kibondo	Nov-Apr	0.37	0.59**	0.50*	-0.03	0.35	0.66 (<0.001)	0.56 (<0.001)
Nkasi	Nov-Apr	0.44*	0.65**	0.53**	0.02	0.42	0.51 (0.017)	0.39 (0.025)
Uvinza	Nov-Apr	0.38	0.61**	0.52**	-0.04	0.37	0.63 (0.002)	0.52 (0.003)
Bimodal districts (MAM and OND seasons)								
Biharamulo	MAM	0.18	-0.11	-0.15	0.21	0.06	0.39 (0.060)	0.38 (0.070)
	OND	0.45*	0.66**	0.54**	0.01	0.43	0.47 (0.022)	0.38 (0.017)
Meatu	MAM	-0.01	-0.28	-0.28	0.04	0.08	0.52 (0.010)	0.57 (0.005)
	OND	0.52*	0.63**	0.44*	0.17	0.41	0.40 (0.057)	0.31 (0.065)
Same	MAM	0.07	-0.12	-0.14	0.10	0.02	0.16 (0.436)	0.17 (0.436)
	OND	0.63**	0.81**	0.67**	0.19	0.66	0.36 (0.074)	0.25 (0.038)

* $q < 0.05$, ** $q < 0.01$ (Benjamini-Hochberg across the eleven series). Year effects are ordinary least-squares coefficients scaled to SPI per decade with their unadjusted *p*-values (FDR-adjusted results are given in the text). DMI was linearly detrended before analysis.



530

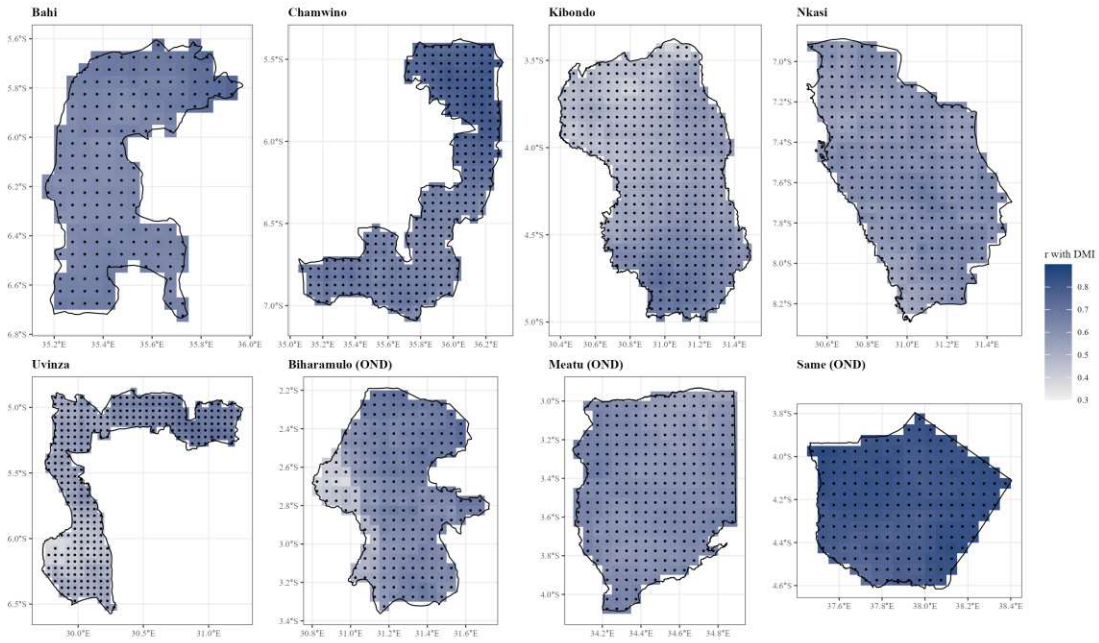
531 **Fig. 9** (a) Correlations of season-matched SPI with ONI, DMI and DMI controlling for ONI (filled
532 symbols: FDR $q < 0.05$). (b) SPI in negative IOD, neutral and positive IOD seasons for the OND and
533 November-April series; bars mark composite means and shading marks SPI ≤ -1.5

534 The modes were statistically associated with part of the temporal change. Three of the five positive
535 IOD years of the record fell in 2018-2023, and adding ONI and DMI to the regression reduced the
536 year coefficient by about 15-30% in the OND and November-April series (Table 7). Nevertheless,
537 the residual year effect remained significant after FDR adjustment in four series (Kibondo, Uvinza,
538 Meatu MAM and Biharamulo OND) and was borderline (q = 0.051-0.053) in Bahi, Chamwino,
539 Nkasi and Same OND. The recent shift towards wetter seasons is therefore partly, but not wholly,
540 associated with the run of positive IOD events.

541 These conclusions were insensitive to the choice of index and method. Using the DMI without
542 detrending gave slightly stronger correlations with OND and November-April SPI (r = 0.67-0.84),
543 so detrending is the conservative choice. Rank (Spearman) correlations were 0.46-0.72 with the
544 DMI against 0.27-0.61 with the ONI. Replacing the ONI with the RONI weakened the ENSO
545 association (r = 0.28-0.58 for the OND and November-April series, significant after FDR
546 adjustment only for Meatu and Same OND), left the partial correlation of SPI with ENSO

controlling for the DMI non-significant in every series (-0.16 to 0.14) and slightly strengthened the DMI association controlling for ENSO (partial r = 0.46-0.69, all $q < 0.05$). The dominance of the IOD therefore does not depend on the ENSO index chosen. Varying the IOD threshold from ±0.4 °C to ±0.3 °C or ±0.5 °C did not change the central result: none of the nine severe or extreme OND and November-April seasons occurred during a positive IOD at any threshold.

The IOD signal was spatially pervasive (Fig. 10). Cell-level correlations of season-matched SPI with the DMI were 0.36-0.85 in the OND and November-April seasons and were significant after field-wide FDR control in 98-100% of cells in every district, with the strongest and most uniform coupling in Same (median $r = 0.81$) and Chamwino (0.68). The weakest values occurred in the northern part of Kibondo, the western edge of Biharamulo and southern Uvinza ($r \approx 0.4$). In the MAM season, no cell in Biharamulo or Same and only 3% of cells in Meatu had a significant correlation, all of them negative.



559

560 **Fig. 10** Grid-cell correlation of season-matched SPI with the detrended September-November DMI for the
561 OND and November-April seasons. Dots mark correlations significant after false-discovery-rate control.
562 MAM is not shown because almost no cell had a significant correlation

563 ## 4 Discussion

564 ### 4.1 Characterising drought across contrasting rainfall regimes

565 A common approach to locating drought hotspots is to compare the frequency of SPI drought
566 classes between sites. Comparing each district's number of severe or extreme droughts with the
567 range expected by chance, and the permutation test, found no evidence that drought frequency
568 differed between the study districts at any of the four timescales. This is expected when each site
569 is standardised against its own climatology: over the reference period all sites have the same
570 expected frequency of each SPI class, and the observed frequencies in a 30-year record differ only
571 within the range expected by chance. This does not mean the districts share the same drought risk.
572 Rather, the information that distinguishes them lies in event structure (duration and persistence),
573 in the co-variability that makes droughts regional, and in the absolute rainfall at stake. One
574 standard deviation of November-April rainfall is similar in Bahi and Kibondo (184 and 171 mm),

yet a season one standard deviation below the mean still receives about 460 mm in Bahi but about 830 mm in Kibondo (Table 3), with very different consequences for crops and water supply. This is consistent with the CLIMATCH classification having been based on crop failure and food insecurity, and with the view that meteorological indices must be combined with exposure and vulnerability to describe drought risk (Carrão et al. 2016). The implications of this distinction for health studies are considered below.

4.2 Interpreting the wetting signal

Estimated SPI trends were positive in all eleven district-seasons over 1995-2024, although only four remained significant after FDR adjustment, and SPI-6 drought months fell by about two-thirds after 2009. The decline is consistent with the partial recovery of the East African long rains since about 2009, after their decline from the late 1990s (Lyon and DeWitt 2012; Wainwright et al. 2019). However, three findings argue against describing it as a robust long-term trend. First, no unimodal trend was significant for windows ending before 2021, and slopes for windows ending in 2015-2019 were close to zero. Second, in four of the five unimodal districts the Pettitt change points fell in 2016-2018, consistent with a recent shift rather than a gradual change, although only the shift in Kibondo was statistically significant. Third, part of the change was statistically associated with the unusual frequency of positive IOD events in 2018-2023, although a residual year effect remained in several series. At the grid-cell scale the direction of change was nonetheless consistent: no cell in any district showed a significant drying trend. The record begins near the 1996-2000 dry spell and ends in a predominantly wet period, both of which steepen the fitted slope. This may also explain the apparent disagreement with Makula et al. (2025), who reported increasing OND drought in parts of Tanzania using SPEI and the Vegetation Health Index for a record ending in 2016, before the recent wet years. Because SPI excludes evaporative demand, a

precipitation-based wetting does not rule out increasing agricultural drought under rising temperatures (Vicente-Serrano et al. 2010; Dai 2013).

4.3 The Indian Ocean Dipole and seasonal drought

The stronger association of OND and November-April SPI with the IOD than with ENSO agrees with modelling and observational work showing that Indian Ocean SST anomalies, rather than ENSO directly, largely control the East African short rains (Black et al. 2003; Behera et al. 2005; Ummenhofer et al. 2009), and with the national-scale association of OND drought with La Niña and negative IOD reported by Makula et al. (2025). Our partial correlations add that, at district scale in Tanzania, ENSO showed no significant association with SPI once the IOD was accounted for, although the correlation between the two modes limits how far their contributions can be separated. This is consistent with the proposal that ENSO influences East African rainfall largely through its effect on the Indian Ocean (Black et al. 2003). The association extends beyond the bimodal short rains: the IOD of the preceding September-November explains between a third and a half (35-54%) of the variance of the November-April season in the unimodal central and western districts, because November-December rainfall is a substantial part of that season (Fig. 2). The absence of any significant link for MAM is consistent with the weak predictability of the long rains (Nicholson 2017).

The asymmetry is relevant to early warning. None of the nine severe or extreme OND and November-April seasons occurred under a positive IOD or El Niño; eight occurred under negative IOD conditions and eight under La Niña conditions. With so few events, this shows an association, not that a positive IOD prevents severe drought. The DMI led monthly SPI-6 by four to five months, which suggests that IOD monitoring and forecasts could give useful warning for

November-April and OND drought in these districts, although the accuracy of such forecasts was not evaluated here.

4.4 Implications for measuring drought exposure in health studies

The districts were selected to study how drought affects the use of healthcare services for diabetes and hypertension, and the results have direct consequences for how drought exposure should be defined in that work. We draw out five implications.

First, drought exposure should be measured as a continuous, season-specific hazard, not as a fixed district label. The CLIMATCH drought-prone classification was not reflected in the frequency of meteorological drought, which was statistically indistinguishable across districts (Table S3 in Online Resource 1), and data-driven groupings of districts cut across it (Fig. 7). Using the label as the exposure would therefore fail to separate the hazard from the vulnerability and baseline conditions that the label was built from, such as aridity, livelihoods and food insecurity. Those conditions also influence the use of diabetes and hypertension services independently, through poverty, distance to facilities and differences in diet and disease prevalence, so the label is likely to be misclassified (Armstrong 1998) as well as confounded. A more informative design treats season-matched SPI as the time-varying exposure and district vulnerability as a separate, time-invariant modifier. An interaction between SPI and district type then tests directly the hypothesis implied above: that the same standardised deficit has a larger effect on service use in semi-arid districts such as Bahi and Chamwino than in wetter districts such as Kibondo.

Second, because drought frequency is similar across districts, the information needed to estimate effects on service use lies in variation over time within districts, not in comparisons between them. Designs with district or facility fixed effects, which compare drought and non-drought periods within the same district or facility, use this variation and remove stable differences in population,

643 access and reporting. Two features of the drought record make control for time essential. Drought
644 is regionally coherent, so drought seasons tend to occur in several districts at once and coincide
645 with national events such as food price shocks. More importantly, drought became markedly less
646 frequent after 2009. Any change in service use over the same period for reasons unrelated to
647 climate, such as changes in health services or in how visits are recorded, would then appear as an
648 association with drought. Adjustment for secular trends, for example with year effects or flexible
649 time terms, is therefore essential.

650 Third, the timescale and timing of exposure should follow the rainy season and the pathway to
651 service use. Drought may reduce routine clinic attendance and medicine refills when household
652 income falls and travel becomes more costly, and may increase visits for poorly controlled disease
653 through food insecurity, changes in diet, heat and psychological stress; analyses should therefore
654 allow for effects in either direction and, where possible, separate routine follow-up visits from
655 visits for complications. Season-end SPI integrates rainfall over the season that determines
656 harvests and household income, so monthly service records are best linked to the SPI of the
657 preceding season with lags covering the following months, including the lean season. In the
658 bimodal districts the two seasons should be treated as separate exposures: MAM and OND SPI
659 were only weakly correlated (r = 0.13-0.34), and only OND drought was linked to the IOD. Where
660 the question concerns prolonged or cumulative exposure, the run-theory event measures (duration,
661 severity and onset) derived from monthly SPI-6 provide a complementary exposure, and their
662 consistency across SPI-3, SPI-6 and SPI-12 (Table S1 in Online Resource 1) indicates that
663 conclusions should not depend strongly on the accumulation period chosen.

664 Fourth, the recent wet period limits statistical power for recent health data. Eleven seasons reached
665 severe or extreme drought in 1995-2009 but none did in 2010-2024, and moderate-or-worse

seasons fell from 35 to 11. Routine health information systems in Tanzania cover mainly this recent, wetter period, so analyses restricted to severe drought would have almost no exposed seasons. Continuous SPI, or thresholds at moderate drought (SPI ≤ -1.0), will be needed to retain contrast, and the absence of recent severe droughts should be reported as a limitation of exposure range rather than read as evidence that drought does not affect service use.

Fifth, district-mean SPI is a reasonable starting exposure, and periods of high drought risk may be anticipated. The grid-cell analysis showed that the direction of change was uniform within districts, except in Same MAM, although its strength and significance varied (Fig. 8). District-mean SPI is therefore a reasonable exposure for service data recorded at district or facility level, whereas grid-cell SPI is preferable where facilities can be located within districts, particularly in parts of districts where change was weaker, such as western Biharamulo. The IOD explained 35-65% of the interannual variance of OND and November-April SPI and led monthly SPI-6 by four to five months, so IOD monitoring and forecasts could help health services prepare, for example by securing stocks of antidiabetic and antihypertensive medicines, offering longer prescription refills or organising outreach clinics before an expected drought season, although the accuracy of such forecasts for these districts remains to be tested.

4.5 Limitations

Drought was characterised from precipitation alone. The Standardized Precipitation Evapotranspiration Index (SPEI) (Vicente-Serrano et al. 2010) or soil-moisture indices could complement SPI by capturing evaporative demand and soil-water deficits, and vegetation indices could help link meteorological drought to agricultural impacts. CHIRPS performance may be reduced in complex terrain (Dinku et al. 2018), such as the mountainous parts of Same, and district averages may hide variation in drought exposure within districts. The short record, with 29-30

seasonal values and 10-17 drought events per district, limits the precision of return-period estimates for rare events and of the regression estimates of trends and climate-mode associations. This uncertainty was assessed with bootstrap confidence intervals and with the sensitivity of trends to the analysis period, but it remains substantial, particularly for rare events. The recommendations for drought exposure assessment are derived from the meteorological record alone and have not yet been tested against the use of diabetes and hypertension services. Because drought years are shared between districts, drought counts are not independent across districts; this makes the permutation test conservative, that is, less likely to detect real differences between districts, although the district-by-district comparison with the binomial range is not affected.

The eight districts were purposively selected and do not represent drought patterns across all of Tanzania. Finally, the CLIMATCH district groups were defined mainly from drought impacts and vulnerability rather than from meteorological hazard, so our findings neither validate nor invalidate that classification for its intended purpose.

5 Conclusions

This study characterised meteorological drought in eight Tanzanian districts with contrasting rainfall regimes over 1995-2024 across multiple timescales, seasons and spatial scales. Four findings stand out. First, no significant differences in standardised drought frequency were detected between districts, including between districts previously classified as drought-prone and non-drought-prone. What distinguishes districts appears to be event structure, the rainfall at stake and vulnerability, rather than how often standardised deficits occur. Second, drought was regionally coherent, with widespread events in 1996-2000, 2003-2006 and 2016-2017. Third, estimated SPI trends were positive in all eleven district-seasons and drought months fell by 68% after 2009, but only four trends remained significant after FDR adjustment, and the wetting signal

depended largely on the predominantly wet years 2019-2024; no grid cell showed a significant drying trend. Fourth, the Indian Ocean Dipole was more strongly associated with October-December and November-April drought than ENSO, which showed no significant independent association, and no severe or extreme drought season in the record occurred under a positive IOD, although such events were few.

For research on drought and the use of diabetes and hypertension services in these districts, the results recommend continuous, season-matched SPI as the exposure rather than a binary drought-prone label; estimation of effects from variation within districts over time, with explicit control for secular trends; separate treatment of the two seasons in bimodal districts; and continuous or moderate-threshold exposures to retain contrast in the wetter recent period. The value of IOD forecasts for anticipating drought and preparing health services remains to be tested. The season-matched SPI series and event measures produced here provide the drought exposure data for the CLIMATCH health analyses, and the framework can be used in other data-scarce settings where drought and health are studied together.

References

Armstrong BG (1998) Effect of measurement error on epidemiological studies of environmental and occupational exposures. Occup Environ Med 55:651–656. https://doi.org/10.1136/oem.55.10.651

Beguería S, Vicente-Serrano SM, Reig F, Latorre B (2014) Standardized precipitation evapotranspiration index (SPEI) revisited: parameter fitting, evapotranspiration models, tools, datasets and drought monitoring. Int J Climatol 34:3001–3023. https://doi.org/10.1002/joc.3887

Behera SK, Luo J-J, Masson S, et al (2005) Paramount Impact of the Indian Ocean Dipole on the East African Short Rains: A CGCM Study. Journal of Climate 18:4514–4530. https://doi.org/10.1175/JCLI3541.1

Benjamini Y, Hochberg Y (1995) Controlling the False Discovery Rate: A Practical and Powerful Approach to Multiple Testing. Journal of the Royal Statistical Society Series B: Statistical Methodology 57:289–300. https://doi.org/10.1111/j.2517-6161.1995.tb02031.x

Berman JD, Ebisu K, Peng RD, et al (2017) Drought and the risk of hospital admissions and mortality in older adults in western USA from 2000 to 2013: a retrospective study. Lancet Planet Health 1:e17–e25. https://doi.org/10.1016/S2542-5196(17)30002-5

Black E, Slingo J, Sperber KR (2003) An Observational Study of the Relationship between Excessively Strong Short Rains in Coastal East Africa and Indian Ocean SST. Mon Weather Rev 131:74–94. https://doi.org/10.1175/1520-0493(2003)131%3C0074:AOSOTR%3E2.0.CO;2

Carrão H, Naumann G, Barbosa P (2016) Mapping global patterns of drought risk: An empirical framework based on sub-national estimates of hazard, exposure and vulnerability. Global Environmental Change 39:108–124. https://doi.org/10.1016/j.gloenvcha.2016.04.012

Dai A (2013) Increasing drought under global warming in observations and models. Nat Clim Chang 3:52–58. https://doi.org/10.1038/nclimate1633

Dinku T, Funk C, Peterson P, et al (2018) Validation of the CHIRPS satellite rainfall estimates over eastern Africa. Q J R Meteorol Soc 144:292–312. https://doi.org/10.1002/qj.3244

Funk C, Peterson P, Landsfeld M, et al (2015) The climate hazards infrared precipitation with stations—a new environmental record for monitoring extremes. Sci Data 2:150066. https://doi.org/10.1038/sdata.2015.66

Guttman NB (1999) Accepting the standardized precipitation index: a calculation algorithm. J Am Water Resour Assoc 35:311–322. https://doi.org/10.1111/j.1752-1688.1999.tb03592.x

Hamed KH, Rao A (1998) A modified Mann-Kendall trend test for autocorrelated data. Journal of Hydrology 204:182–196. https://doi.org/10.1016/S0022-1694(97)00125-X

Hijmans RJ (2025) terra: spatial data analysis. R package version 1.8-54. https://doi.org/10.32614/CRAN.package.terra

Hosking JRM (1990) L-Moments: Analysis and Estimation of Distributions Using Linear Combinations of Order Statistics. Journal of the Royal Statistical Society Series B: Statistical Methodology 52:105–124. https://doi.org/10.1111/j.2517-6161.1990.tb01775.x

Huang B, Yin X, Boyer T, et al (2025) Extended Reconstructed Sea Surface Temperature, Version 6 (ERSSTv6). Part I: An Artificial Neural Network Approach. Journal of Climate 38:1105–1121. https://doi.org/10.1175/JCLI-D-23-0707.1

Kendall MG (1975) Rank Correlation Methods, 4th edn. Charles Griffin, London

Lyon B, DeWitt DG (2012) A recent and abrupt decline in the East African long rains. Geophysical Research Letters 39:L02702. https://doi.org/10.1029/2011GL050337

Makula EK, Mangara RJ, Kazimili B, et al (2025) Assessment of drought characteristics using SPEI and VHI in Tanzania and their associated climate factors. Nat Hazards 121:2071–2093. https://doi.org/10.1007/s11069-024-06894-6

775 Mann HB (1945) Nonparametric Tests Against Trend. Econometrica 13:245–259.
776 https://doi.org/10.2307/1907187

777 McKee TB, Doesken NJ, Kleist J (1993) The relationship of drought frequency and duration to
778 time scales. In: Eighth Conference on Applied Climatology. American Meteorological
779 Society, Boston, MA, pp 179–184

780 Mishra AK, Singh VP (2010) A review of drought concepts. Journal of Hydrology 391:202–216.
781 https://doi.org/10.1016/j.jhydrol.2010.07.012

782 Moreira RP, Da Silva CBC, De Sousa TC, et al (2024) The Influence of Climate, Atmospheric
783 Pollution, and Natural Disasters on Cardiovascular Diseases and Diabetes Mellitus in
784 Drylands: A Scoping Review. Public Health Rev 45:1607300.
785 https://doi.org/10.3389/phrs.2024.1607300

786 Mukama EB, Yimer EA, Mbungu WB, et al (2025) Evaluating the standardized and threshold
787 based drought indices for historical drought detection in the Great Ruaha River Basin,
788 Tanzania. Nat Hazards 121:12243–12273. https://doi.org/10.1007/s11069-025-07279-z

789 Muthoni FK, Odongo VO, Ochieng J, et al (2019) Long-term spatial-temporal trends and
790 variability of rainfall over Eastern and Southern Africa. Theor Appl Climatol 137:1869–
791 1882. https://doi.org/10.1007/s00704-018-2712-1

792 Nicholson SE (2017) Climate and climatic variability of rainfall over eastern Africa. Reviews of
793 Geophysics 55:590–635. https://doi.org/10.1002/2016RG000544

794 NOAA NWS (2026) Implementing a Relative Oceanic Niño Index effective February 1, 2026.
795 https://weather.gov/media/notification/pdf_2026/pns26-05_Relative_ONI.pdf. Accessed
796 26 Oct 2026

797 Pebesma E (2018) Simple Features for R: Standardized Support for Spatial Vector Data. The R
798 Journal 10:439–446. https://doi.org/10.32614/RJ-2018-009

799 Pettitt AN (1979) A Non-Parametric Approach to the Change-Point Problem. Applied Statistics
800 28:126–135. https://doi.org/10.2307/2346729

801 Pohlert T (2023) trend: non-parametric trend tests and change-point detection. R package version
802 1.1.6. https://doi.org/10.32614/CRAN.package.trend

803 Rayner NA, Parker DE, Horton EB, et al (2003) Global analyses of sea surface temperature, sea
804 ice, and night marine air temperature since the late nineteenth century. J Geophys Res
805 108:4407. https://doi.org/10.1029/2002JD002670

806 Saji NH, Goswami BN, Vinayachandran PN, Yamagata T (1999) A dipole mode in the tropical
807 Indian Ocean. Nature 401:360–363. https://doi.org/10.1038/43854

808 Salah M, Moursy F, Soliman E, Gamal G (2023) Assessing the potential impacts of climate change
809 on droughts in East Africa using CORDEX-CORE regional climate models' simulations:

A focus on Tanzania. Contrib Geophys Geod 53:271–300. https://doi.org/10.31577/congeo.2023.53.3.6

Salvador C, Nieto R, Vicente-Serrano SM, et al (2023) Public Health Implications of Drought in a Climate Change Context: A Critical Review. Annu Rev Public Health 44:213–232. https://doi.org/10.1146/annurev-publhealth-071421-051636

Sen PK (1968) Estimates of the Regression Coefficient Based on Kendall's Tau. Journal of the American Statistical Association 63:1379–1389. https://doi.org/10.1080/01621459.1968.10480934

Şen Z (2012) Innovative Trend Analysis Methodology. J Hydrol Eng 17:1042–1046. https://doi.org/10.1061/(ASCE)HE.1943-5584.0000556

Shiau JT (2006) Fitting Drought Duration and Severity with Two-Dimensional Copulas. Water Resour Manag 20:795–815. https://doi.org/10.1007/s11269-005-9008-9

Stagge JH, Tallaksen LM, Gudmundsson L, et al (2015) Candidate distributions for climatological drought indices (SPI and SPEI). Int J Climatol 35:4027–4040. https://doi.org/10.1002/joc.4267

Stanke C, Kerac M, Prudhomme C, et al (2013) Health Effects of Drought: a Systematic Review of the Evidence. PLoS Curr 5:ecurrents.dis.7a2cee9e980f91ad7697b570bcc4b004. https://doi.org/10.1371/currents.dis.7a2cee9e980f91ad7697b570bcc4b004

Svoboda M, Hayes M, Wood D (2012) Standardized Precipitation Index User Guide. World Meteorological Organization, Geneva

TMA (2025) Statement on the status of Tanzania climate in 2024. https://www.meteo.go.tz/uploads/documents/sw-1758111343-Tanzania%20Climate%20Statement%202024.pdf. Accessed 26 Oct 2026

Ummenhofer CC, Sen Gupta A, England MH, Reason CJC (2009) Contributions of Indian Ocean Sea Surface Temperatures to Enhanced East African Rainfall. Journal of Climate 22:993–1013. https://doi.org/10.1175/2008JCLI2493.1

Van Loon AF (2015) Hydrological drought explained. WIREs Water 2:359–392. https://doi.org/10.1002/wat2.1085

Venables WN, Ripley BD (2002) Modern Applied Statistics with S, 4th edn. Springer New York, New York, NY

Vicente-Serrano S, Beguería S, López-Moreno JI (2010) A Multiscalar Drought Index Sensitive to Global Warming: The Standardized Precipitation Evapotranspiration Index. Journal of Climate 23:1696–1718. https://doi.org/10.1175/2009JCLI2909.1

Vins H, Bell J, Saha S, Hess J (2015) The Mental Health Outcomes of Drought: A Systematic Review and Causal Process Diagram. Int J Environ Res Public Health 12:13251–13275. https://doi.org/10.3390/ijerph121013251

Wainwright CM, Marsham JH, Keane RJ, et al (2019) 'Eastern African Paradox' rainfall decline due to shorter not less intense Long Rains. npj Clim Atmos Sci 2:34. https://doi.org/10.1038/s41612-019-0091-7

Wainwright CM, Finney DL, Kilavi M, et al (2021) Extreme rainfall in East Africa, October 2019–January 2020 and context under future climate change. Weather 76:26–31. https://doi.org/10.1002/wea.3824

Wambura FJ (2025) Effects of Inconsistency in Drought Event Definitions on Drought Characteristics. Hydrology 12:26. https://doi.org/10.3390/hydrology12020026

Wickham H (2016) ggplot2: elegant graphics for data analysis. Springer International Publishing, Cham

Wilhite DA, Glantz MH (1985) Understanding the Drought Phenomenon: The Role of Definitions. Water Int 10:111–120. https://doi.org/10.1080/02508068508686328

Wilks DS (2016) "The Stippling Shows Statistically Significant Grid Points": How Research Results are Routinely Overstated and Overinterpreted, and What to Do about It. Bulletin of the American Meteorological Society 97:2263–2273. https://doi.org/10.1175/BAMS-D-15-00267.1

Yan J (2007) Enjoy the Joy of Copulas: With a Package **copula**. J Stat Softw 21:1–21. https://doi.org/10.18637/jss.v021.i04

Yevjevich V (1967) An objective approach to definitions and investigations of continental hydrologic droughts. Colorado State University, Fort Collins

Statements and Declarations

Funding

This study was conducted as part of the corresponding author's PhD studies, funded by the Ministry of Foreign Affairs of Denmark through the Danida Fellowship Centre (DFC; file no. 23-03-RH) as part of the CLIMATCH project.

Competing interests

The authors declare that they have no competing interests.

Author contributions

Elia Magwaja conceptualised the study, analysed the data, drafted the manuscript and compiled the final version. Peter Tuju, Habiba Mtongori and Jim Todd provided analytical support, reviewed and edited the manuscript. Anthony Kapesa, George PrayGod, Brenda Kitilya, Eliud Kamala, Eliakimu Kapyolo, Daniel Faurholt-Jepsen, Zvifadzo Matsena Zingoni and Ladislaus Chang'a reviewed the manuscript and provided critical comments. All authors read and approved the final manuscript.

Data availability

The datasets analysed in this study are available as follows:

Rainfall: Climate Hazards Group InfraRed Precipitation with Station data (CHIRPS), version 2.0, Climate Hazards Center, University of California, Santa Barbara; https://doi.org/10.15780/G2RP4Q.

ENSO: Oceanic Niño Index (ONI) and Relative Oceanic Niño Index (RONI), NOAA Climate Prediction Center; https://www.cpc.ncep.noaa.gov/data/indices/oni.ascii.txt and https://www.cpc.ncep.noaa.gov/data/indices/RONI.ascii.txt.

IOD: Dipole Mode Index (DMI) based on HadISST1.1, NOAA Physical Sciences Laboratory; https://psl.noaa.gov/data/timeseries/month/DMI/.

District rainfall series: the district-mean daily rainfall series were extracted from CHIRPS by the Tanzania Meteorological Authority (TMA) and are not publicly available because they are held under TMA's data policy; they are available from TMA on request.

No new datasets were generated in this study.

Ethics approval

Not applicable.

Supplementary Files

This is a list of supplementary files associated with this preprint. Click to download.

- ESM1.pdf